Title

Aging-associated changes in cerebral vasculature and blood flow as determined by quantitative optical coherence tomography angiography

Authors

Li, Yuandong
Choi, Woo June
Wei, Wei
et al.

Publication Date

2018-10-01

DOI

10.1016/j.neurobiolaging.2018.06.017

Peer reviewed

HHS Public Access

Author manuscript

Neurobiol Aging. Author manuscript; available in PMC 2019 October 01.

Published in final edited form as:

Neurobiol Aging. 2018 October ; 70: 148–159. doi:10.1016/j.neurobiolaging.2018.06.017.

Aging-associated changes in cerebral vasculature and blood flow as determined by quantitative optical coherence tomography angiography

Yuandong Li[#1], **Woo June Choi**[#1,2], **Wei Wei**[1], **Shaozhen Song**[1], **Qinqin Zhang**[1], **Jialing Liu**[3], and **Ruikang K. Wang**[1,*]

[1]Department of Bioengineering, College of Engineering and School of Medicine, University of Washington, Seattle, WA 98195, USA

[2]School of Electrical and Electronics Engineering, College of ICT Engineering, Chung-Ang University, Seoul, 06974, Korea

[3]Department of Neurological Surgery, University of California, San Francisco and SFVAMC, San Francisco, CA 94118, USA

[#] These authors contributed equally to this work.

Abstract

Normal aging is associated with significant alterations in brain's vascular structure and function, which can lead to compromised cerebral circulation and increased risk of neurodegeneration. The *in vivo* examination of cerebral blood flow (CBF), including capillary beds, in aging brains with sufficient spatial detail remains challenging with current imaging modalities. In the present study, we use threedimensional (3-D) quantitative optical coherence tomography angiography (OCTA) to examine characteristic differences of the cerebral vasculatures and hemodynamics at the somatosensory cortex (S1) between old (16-month-old) and young mice (2-month-old) *in vivo*. The quantitative metrics include cortical vascular morphology, CBF, and capillary flow velocity. We show that compared to young mice, the pial arterial tortuosity increases by 14%, the capillary vessel density decreases by 15%, and the CBF reduces by 33% in the old mice. Most importantly, changes in capillary velocity and heterogeneity with aging are quantified for the first time with

[*]Corresponding author: wangrk@uw.edu, Address: 3720 15th Ave NE, N415A, Seattle, WA 98195.

Conflicts of Interest

Dr. Wang discloses intellectual property owned by the Oregon Health and Science University and the University of Washington related to OCT angiography, and licensed to commercial entities, related to the technology and analysis methods described in parts of this manuscript. The other authors have no conflicts of interest to declare.

Animal research

All animal experimental procedure in this study were approved by the Institutional Animal Care and Use Committee (IACUC) of the University of Washington and conduced in accordance with University of Washington guidelines.

Other verifications

The data contained in this manuscript being submitted have not been previously published, and have not been submitted elsewhere and will not be submitted elsewhere while under consideration at Neurobiology of Aging.

All authors have reviewed the contents of the manuscript being submitted. The contents and data are approved by all authors.

sufficiently high statistical power between young and old populations, with a 21% ($p<0.05$) increase in capillary mean velocity and 19% ($p\leq0.05$) increase in velocity heterogeneity in the latter. Our findings through non-invasive imaging are in line with previous studies of vascular structure modification with aging, with additional quantitative assessment in capillary velocity enabled by advanced OCTA algorithms on a single imaging platform. The results offer OCTA as a promising neuroimaging tool to study vascular aging, which may shed new light on the investigations of vascular factors contributing to the pathophysiology of age-related neurodegenerative disorders.

Keywords

optical coherence tomography angiography; capillary imaging; aging; neurodegeneration; Alzheimer's disease; tortuous blood vessel; capillary loss; cerebral blood flow; capillary transit time heterogeneity

1. INTRODUCTION

Normal aging is associated with modifications to the biomechanical properties of blood vessels, which can result in anatomical and functional alterations in the brain vasculatures (Diaz-Otero et al., 2016), and potentially lead to hypoperfusion or neurodegeneration (de la Torre, 1999). Although there is no consensus reached regarding the causal relationship between a decreased cerebral blood flow (CBF) and decline of neuronal function, there is an increasing prevalence of coincident cerebrovascular deficiency and cognitive dysfunction with aging that is also well recognized in Alzheimer's disease (AD) (Attems and Jellinger, 2014; Breteler, 2000; Hofman et al., 1997). Thus, the ability to image cerebral vasculatures with superior spatial detail in the aging brain and to precisely quantify vascular parameters will not only be invaluable to uncover the vascular deficiency associated with normal aging, but also crucial to decipher the functional relationship between cerebrovascular factors and pathological neurodegeneration.

A compromised structural integrity of the cerebral vasculature is a representative degenerative feature of the vascular system in the aging brain (Farkas and Luiten, 2001). Changes in vascular morphology have been identified in early studies by microscopy with post-mortem brain tissue. In larger vessels, for example, increased tortuosity has been observed in the middle, anterior and posterior cerebral arterioles of aging mice (Faber et al., 2011; Kang et al., 2016), and in the penetrating arterioles within the white matter from humans as early as in middle age (Bullitt et al., 2010; Thore et al., 2007). At the level of cerebral microvessels, there are considerable evidences of an age-related reduction in capillary numbers and capillary density in the brain of aged rodents (Amenta et al., 1995; Burns et al., 1981; Casey and Feldman, 1985; Hinds and McNelly, 1982; Jucker et al., 1990; Knox and Oliveira, 1980; Sonntag et al., 1997; Villena et al., 2003; Wilkinson et al., 1981), and a decreased capillary density in older human brains (Abernethy et al., 1993; Bell and Ball, 1981; Brown et al., 2007; Buée et al., 1994; Mann et al., 1986).

The anatomical changes seen in the cerebral vessels may alter the conductance and resistance of the vascular network, leading to reduced CBF or even hypoperfusion in the

cerebral tissue (Xu et al., 2017). Consequently, cerebral metabolism can diminish, which eventually jeopardizes functional neuronal activities (Kisler et al., 2017). A number of clinical studies employing a range of imaging technologies have investigated CBF or arterial flow velocity in healthy aging subjects. Functional magnetic resonance imaging (fMRI) (Ances et al., 2009) and positron emission tomography (PET) (Aanerud et al., 2012) have used to reveal regionally-specific decreases in CBF during functional activity of brain in aging, while transcranial Doppler sonography (Demirkaya et al., 2008) has shown a decrease in blood flow velocity in large cerebral arteries with advancing age. Although these *in vivo* imaging studies have cumulatively found an association between macroscopic perfusion reduction and aging (Berman et al., 1988; Bertsch et al., 2009; Heo et al., 2010; Lynch et al., 1999), changes in microscopic flow remained poorly understood due to their inherent limitations in providing adequate spatial resolution required to assess capillary flow (Wang et al., 2014), in addition to a sufficient penetration depth to image sub-surface cerebral microvessels in a living subject without excessive disruption to the neuronal environment. A recent aging study has attempted to address such challenges by utilizing high-speed two-photon fluorescence microscopy (TPM) to examine age-related differences in cerebral capillary blood flow between young and old rodent brains *in vivo* (Desjardins et al., 2014). Despite outstanding image quality, the very slow speed of data-acquisition and the restricted imaging area (800μm × 800μm) or depth (100 μm below the surface) make the TPM a less ideal tool for imaging cerebral capillary blood flow.

Optical coherence tomography (OCT) has emerged as a non-invasive neuroimaging technique that distinguishes itself from other micrometer-scale resolution imaging techniques with a significant speed advantage in 3-D imaging and an appreciable penetration depth, typically at ≥1 mm in tissue (Choi et al., 2016). Furthermore, recent advances in OCT angiography (OCTA) techniques, such as the development of optical microangiography (OMAG) (Wang et al., 2007), have allowed for the acquisition of blood flow information from the volumetric OCT dataset down to the capillary level by coherently analyzing the intrinsic scattering property of moving RBCs in functioning blood vessels. Furthermore, Doppler OMAG (DOMAG) (Shi et al., 2013) has been developed to quantitatively measure RBC moving velocity via the axial component and to evaluate penetrating arterioles (PA) flow dynamics in the cerebral cortex (Baran et al., 2015). In addition to quantitative assessment of arteriole blood flow, we have recently developed an eigen-decomposition (ED) analysis of the complex optical signals generated by high-speed OCTA scans to extract the frequency components of single-file moving RBC in capillary passages (Wang et al., 2017). A statistical evaluation of a large quantity (thousands) of capillary velocities in 3-D tissue volumes at 50 μs temporal resolution provides a glimpse of capillary flow heterogeneity in the region of interest (Li et al., 2018).

In this study, we employed a combination of OCTA techniques to examine the age-related vascular and blood flow changes in the cerebral cortex of anesthetized mice *in vivo* using a single imaging platform. The effect of aging on cerebral vessel structure and *in vivo* flow dynamics is quantitatively characterized using OCTA measurement parameters of vessel tortuosity and density, CBF, capillary velocity and heterogeneity.

2. METHOD AND MATERIALS

2.1 Animal preparation

All experimental procedures in this study performed on animals were approved by the Institutional Animal Care and Use Committee (IACUC) of the University of Washington. Young (2-month-old, n=8) and old (16-month-old, n=8) male C57BL/6 mice (Charles River Laboratory) were used. Females were not included due to potential influence of hormonal fluctuation on blood flow. Mice were housed in individual cages at the imaging facility for at least 1 week prior to experimentation on a 12/12-hour light/dark cycle with access to food and water ad libitum.

On the day of the experiment, mice were anesthetized with isoflurane and placed on a stereotaxic frame (51625, Stoelting Co.) for head stabilization. Isoflurane was continuously being delivered to the animal with a mixture of 0.2 L/min pure oxygen and 0.8 L/min air. Each mouse received an open skull cranial window surgery (Li et al., 2014), where a 4.5-mm-diameter round craniotomy at the somatosensory cortex (S1) region (1 mm posterior and lateral to the bregma) was performed on the right parietal bone as shown in an inset of Fig. 1. In this procedure (Li et al., 2014), a circular piece of skull was carefully detached and replaced with a round, transparent glass coverslip measuring 5 mm in diameter. Cyanoacrylate glue was used to seal the glass coverslip to the skull, yielding a 4-mm-diameter flat cortex surface as an imaging window. The entire cranial window was subjected to OCT imaging with dedicated scanning protocols in section 2.3. Physiological parameters of the animal were monitored, including anesthesia depth, blood pressure (CODA Surgical Monitor, Kent Scientific Corp.), as well as body temperature (507223F, Harvard Apparatus) throughout the experiments, before then being euthanized by cervical dislocation.

2.2 OCT system configuration

An in-house-built, 1300 nm high-speed spectral-domain OCT (SD-OCT) system (Fig. 1) was employed for *in vivo* imaging of mouse cerebral cortex (Wang and An, 2009). The system was equipped with a broadband super-luminescent diode (SLD) light source (LS2000B, Thorlabs Inc.) with a center wavelength of 1349 nm and a spectral bandwidth of ~110 nm at 3dB, providing a measured axial resolution of ~7 μm in air (~5.1 μm in mouse brain tissue). In the sample arm, a 10× objective lens (LSM02, Thorlabs Inc.) focused the light beam into the cerebral cortex through the cranial window, giving a lateral resolution of ~10 μm. The light reflected from the sample interfered with the reference light, which was then spectrally detected by a custom spectrometer consisting of a transmission grating, an achromatic double lens, and a 1024-pixel InGaAs line scan camera operated at 92,000 axial scans per second. The light beam was scanned over the cranial window using a paired X-Y galvo scanners (6210H, Cambridge Technology), yielding 3-D volumetric data set (z-x-y). The system sensitivity was measured to be 105 dB at the focus (~500 μm below the zero delay line) with an incident light power of ~5 mW at the sample. A visible light (633 nm He-Ne laser) was coupled to the system to aid in targeting the scanning regions.

2.3 OCTA scanning protocols

Three scanning protocols were employed at single imaging session for different types of blood flow analysis as described below.

2.3.1 OMAG—OMAG scanning protocol (Wang et al., 2007) is used to image the morphological features of cerebral blood vessel networks. In this protocol, each B-frame consisted of 400 A-lines (z axis) covering a distance of ~2.5 mm in the transverse direction (x axis). B-frame was repeated 8 times at each transverse location, and a total of 400 locations was recorded in the C-scan direction (y axis) covering a distance of ~2.5 mm. Therefore, the final 3-D volumetric dataset consisted of 3200 B-frames, which took ~15 s to acquire at A-scan rate of 72 kHz and B-frame rate of 180 frames/sec (fps). This protocol was performed on four quadrants, and the final image (4mm × 4mm) was automatically stitched from 4 angiograms with ~1 mm overlap.

2.3.2 DOMAG—DOMAG scanning protocol (Shi et al., 2013) is used to image axial velocity components of cerebral blood flows, particularly in penetrating vessels. This protocol was performed with 25 A-lines repeatedly acquired at each depth location to give one M-scan (z axis). A B-frame consisted of 300 M-scans covering ~2 mm (x axis), and a total of 300 B-frames (y axis) covering ~2 mm was captured to accomplish the 3-D dataset. The total scanning time of each dataset is ~50 s at A-scan rate of 45 kHz and B-frame rate of 6 fps. This protocol was performed on 9 tiles over the cranial window to produce the final stitched bidirectional flow velocity map (5mm × 5mm).

2.3.3 OCTA capillary velocimetry—This protocol (Wang et al., 2017) is used to image heterogeneous properties of capillary hemodynamics within scanned tissue beds. In this protocol, we set the A-scan rate to be 20 kHz with 50 A-line performed consecutively at each M-scan position. This setting yields adjustable A-line interval time from 50 μs to 2.5 ms to potentially analyze slow to fast capillary flows from 100 μm/s to 5 mm/s. A B-frame consisted of 200 M-scans covering ~1.5 mm (x axis). A total of 200 B-frames covering ~1.5 mm (y axis) was acquired to finish off the 3-D dataset. The total time to complete one 3-D dataset is ~ 100 s. This protocol was performed at two selected regions inside the cranial window, one region was proximal to the middle cerebral artery (MCA), and the other proximal to anterior cerebral artery (ACA).

2.4 Data analysis

Multiple flow parameters were derived from the OCTA datasets acquired using different scanning protocols on a single OCT platform. The methods used for measuring these vascular parameters, are described as below. All analyses were performed in Matlab (Mathworks, MA, USA) using in-house-designed codes.

2.4.1 Arterial tortuosity measurement—Vessel tortuosity index (VTI) was used to evaluate vessel tortuosity, which is defined as an arc-chord ratio (Hutchins et al., 1978), i.e. the ratio of a length of curved vessel (arc) to a distance of straight line (chord) between the end points of a vessel segment (Fig. 2(a)). In this analysis, segments MCA and ACA were chosen, referred to as arteriolo-arteriolar anastomosis (AAA), for collateral tortuosity

comparison between young and old population. Our choice of AAA is rationalized by the frequent development of collateral vessel tortuosity being reported in normal aging (Faber et al., 2011). A manual segmentation was performed from 3-D OMAG angiograms to show pial vessels within 50-μm-thick slab from cortical surface followed by a binary processing to obtain the vessel skeleton. In a representative 5-pixel skeletonized vessel centerline (Figure 2(b)), chord length was simply the Euclidean distance (yellow dashed line) between two end-point pixels, whereas the arc length was obtained by summing distance of horizontally/vertically and diagonally connected pixels using pixel connectivity method (Efford, 2000), which describes the way in which pixels relate to their neighbors. In this method, the horizontally and vertically connected pixels are identified as 4-neighborhood pixels, whereas the diagonally connected pixels are regarded as 8-neighborhood pixels. For an example, the vessel segment in Fig. 2b returns pixel paths of 3 and 1 for 4-neighborhood (Fig. 2(c)) and 8-neighborhood (Fig. 2(d)), respectively. The resulting arc length can be calculated by: (differences of pixel path number between 4- and 8-neighborghoods) × √2 + total pixel number – pixel path number for 4-neighborhood, that is ((3–1)×√2)+5–3 =4.8. Finally, the VTI was calculated by arc/chord ratio, having a minimum value of 1 (i.e. if VTI = 1, the vessel is straight).

2.4.2 Capillary vessel density quantification—We calculated vessel area density (VAD), defined as the percentage of area occupied by vessels (Chu et al., 2016; Kim et al., 2016), of the capillary network obtained from OMAG angiogram. This parameter calculation was developed previously within our group and validated in ophthalmic imaging for retinal VAD measurements (Chu et al., 2016). To more accurately evaluate cerebral capillary VAD, we reconstructed the 3-D OMAG dataset to segment a 300-pm-thick slab of vessels from the cortical surface, avoiding biased measurements at deeper cortical layers due to multiple-scattering that might cause signal attenuation and resolution degradation. Additionally, large pial vessels (>50 um in diameter) from the *en face* image were excluded. Therefore, individual capillaries within the reconstructed 3-D image were resolvable. The image was then processed into a binary image using global thresholding, a hessian filter, and adaptive thresholding to generate a binary vessel area map, where a value of 1 represents a white pixel, i.e. the presence of a capillary vessel, and 0 the black pixel, i.e. the absence of a functioning vessel (Chu et al., 2016). Finally, the VAD was calculated as a ratio of the area occupied by vessels to a given region (2.5mm × 2.5mm selected).

2.4.3 CBF analysis—Penetrating arterioles (PA) pass blood directly from the pial vessel network and remains uncollateralized, which vertically descend into the cortex tissue and return as rising venules (RV) to the pial network (Nishimura et al., 2007). We evaluated CBF in both arterioles and venules from 3-D DOMAG velocity maps. In this method, firstly, the axial velocity of PA/RV found by phase-based methods utilizing the well-known Doppler effect (Shi et al., 2013; Wang and An, 2009). From the 3-D velocity dataset, an x-y orthogonal slice ~50 μm below the cortex surface was selected from the 3-D dataset to evaluate flow cross sections. Next, regional CBF was obtained by velocity × flow area for each type of vessels measured within 3.5 mm × 3.5 mm region. The values were than normalized to a unit region (1 mm^2) and compared between young and old groups. Note that

this CBF measurement is independent of the Doppler angle (Srinivasan et al., 2010; Zhi et al., 2011).

2.4.4 Capillary mean velocimetry and velocity heterogeneity calculation—An eigen decomposition (ED) -based analysis was used to reveal capillary flow velocity within the 3-D tissue volumes (Wang et al., 2017). Briefly, a frequency analysis was firstly obtained using the covariance matrix of grouped A-lines (50 repetitions), with which the eigenvalues and eigenvectors that represent the subsets of the signal markup were calculated. The signals generated by moving RBCs were isolated via an adaptive regression filter to remove the eigen components that represent static tissue, whereas the frequency components of moving RBC were calculated through first lag-one autocorrelation of the obtained eigenvectors. Then, the capillary flow speed was obtained according to a linear relationship between measured frequency and RBC velocity (Wang et al., 2017). For a more accurate evaluation of capillary velocity and heterogeneity, additional segmentation was performed on each B-frame to remove vessels with lumen larger than 15 μm in diameter. Lastly, capillary mean velocity and velocity heterogeneity within the scanned tissue volume were obtained by calculating the mean and the standard deviation, respectively, from all capillaries in the 3-D dataset.

2.5 Statistical analysis

The differences between young (n=8) and aged (n=8) group were statistically tested using Student *t* tests (two-tailed) for each variable presented in this study. $p<0.05$ was considered statistically significant.

3. RESULTS

3.1 Measured physiology parameters

The mean recorded heart rate, respiratory rate, arterial blood pressure (diastolic and systolic), as well as blood oxygen saturation level (SpO_2) are shown in Table 1. Respiratory rate and SpO_2 levels were not significantly different between young and aged groups, but the heart rate was 10% lower and arterial pressure (both systolic and diastolic) was 11% lower in the older animals at statistically significant level of $p<0.05$

3.2 Arterial tortuosity

OMAG angiograms shown for young (Fig. 3(a)) and old mice (Fig. 3(b)) are of mostly pial vessel networks obtained within 50-μm-thick slab from cortical surface (Fig. 3(c)). The average VTI value measured from the 9 AAA segments in young group (Fig. 3(d)) was 1.19±0.07, whereas the mean value for the aged group (Fig. 3(e)) was 1.36±0.09. The VTI of AAA in old mice is 14% statistically significant higher than that of the young group ($p<0.01$) (Fig. 3(f)), indicating that the collateral vessels at in the older mice are more tortuous.

3.3 Capillary vessel density

Differences in the capillary vessel density between young and old mice were qualitatively revealed by OMAG angiograms and quantified by VAD parameter. In comparison with the

light microscopic images (Fig. 4(a), 4(b)), which show larger surface arterioles only, the OMAG angiograms (Fig. 4(c), 4(d)) reveal high resolution cerebral microvascular networks down to the capillary level. Comparing the angiograms, it is apparent that the older mouse had an uneven distribution of vascular perfusion, where localized rarefaction of capillary perfusion can be seen (Fig. 4(d)). The distribution of VAD is more heterogeneous in the old mice (Fig. 4(f)) compared to the young (Fig. 4(e)). Frequency histogram distribution further shows higher population of VAD over the mean for young mice (Fig. 4(g)), and statistical evaluation reveals the VAD of old mice (0.34±0.08) is 15% statistically significant lower than that of young mice (0.40±0.05) at a significant level of $p<0.01$ (Fig. 4(h)).

3.4 CBF measurements from PA flow

Bidirectional blood flow velocity maps were revealed by DOMAG for young and old mice (Fig. 5(a)), and an x-y orthogonal slice from a 3-D dataset (Fig. 5(b)) produces a projection of flow cross sections (Fig. 5(c)). In Fig. 5(c), PA and RV axial velocity projections on x-z plane can be seen as green and red dots. We compared aged related differences in the mean velocity, and flow area, and total flow of both PA and RV within a unit region (1 mm^2) in Fig. 5(d)-(f). For the mean velocity measurement (Fig. 5(d)), the arteriole velocity was measured to be greater than the venule velocity, in both young and old animals. No statistically significant differences were found in penetrating vessel velocity between young and old groups. In general, flow area of venules was larger than arterioles (Fig. 5(e)). The average flow area of PA is decreased by 35% ($p<0.05$) and flow area of RV is decreased by 32% ($p<0.05$) in older animals. In Fig. 5(f), the total flow (mm^3/s) is calculated as velocity (mm/s) × flow area (mm^2). In the old group, there is a 33% statistically significant reduction ($p<0.01$) in PA total flow, and 31% statistically significant reduction ($p<0.01$) in RV total flow. Additionally, no significant differences were found between PA and RV total flow volume in each individual animal.

3.5 Capillary mean velocity and heterogeneity

Standard OMAG angiograms of young (Fig. 6(a)) and old mice (Fig. 6(b)) delineate two regions on each angiogram for velocimetry assessment, one proximal to MCA and the other proximal to ACA. The resulting velocimetry maps of the two selected regions are shown for young (Fig. 6(c), 6(d)) and old mice (Fig. 6(e), 6(f)). Each velocimetry map contains ~40,000 frequency signals within the 3-D tissue volume. The quantification reveals a capillary mean velocity of 1.11±0.17 mm/s in young mice and 1.34±0.23 mm/s in old mice (value taken from mean of both regions). Therefore, the mean capillary velocity is 21% higher in the old group than in the young at difference level of $p<0.05$ (Fig. 6(g)). The standard deviation, which is regarded as velocity heterogeneity was calculated as 0.44±0.07 mm/s and 0.52±0.08 mm/s in young and old mice, respectively, yielding a 19% increase in capillary velocity heterogeneity in the old group ($p\leq0.05$) (Fig. 6(h)).

4. DISCUSSION

4.1 Relevance and result interpretation

Strong evidence has shown that the degeneration of the brain vasculature and reduced blood flow may underlie age-associated decline in neuronal function or cognition, although the

underlying mechanism remains unclear. With a host of novel OCTA imaging algorithms, we quantitatively characterized a series of age-related differences in cerebral vasculature and blood flow *in vivo* with superior spatial detail between healthy young and old mice. A summary of findings is shown in Table 2. Some important changes in aged animals include 14% increase in collateral tortuosity, 15% decrease in capillary density, 33% decrease in arterial CBF, 21% increase in capillary mean velocity and 19% increase in capillary velocity heterogeneity, all at statistically significant levels. We here discuss each characteristic aged-associated changes in details.

4.1.1 Aging-related vessel tortuosity increase—Vascular aging is known to cause progressive deterioration in the cellular structure of the blood vessel wall, subsequently modifying its biomechanical properties and rendering morphological changes within the vessel architecture (Diaz-Otero et al., 2016). One of the most noticeable changes, the development of arteriole tortuosity, has been observed in cerebral cortex and white matters of animal and human brains in both normal aging and age-related pathological conditions (Brown and Thore, 2011). The majority studies on vessel tortuosity were carried out in human brain post-mortem and were focused on the penetrating arterioles of in white matter diseases (Spangler et al., 1994; Thore et al., 2007), with few studies evaluating tortuosity changes during normal vascular aging *in vivo*. Recently, Faber *et al*. reported an increased tortuosity in rodents from measuring pial cerebral arterioles at the bridge of the MCA and ACA branches, known as AAA, in mouse S1 cortex during normal aging. They demonstrated that the average VTI was much higher (1.43) for the aged group (16-month-old) compared to that of the young group (1.22) (3-month-old), leading to a 6-fold higher flow resistance in cerebral collateral vessel in the aged brain (Faber et al., 2011). Our tortuosity measurements of AAA by OCT produced similar VTI values of 1.36±0.09 and 1.19±0.07 for healthy aged (16-month-old) and young mice (2-month-old), respectively (Fig. 3(f)). Previous studies used fixed brain tissue with dilated and filled pial cortical vessels, albeit an elegant technique used to evaluate post mortem brain vasculature, is prone to potential changes in vessel morphology during tissue processing. In contrast, the label-free, *in vivo* nature of OCTA used in this study preserved the native architectures of the blood vessels and increases the fidelity of the VTI analysis. Apart from methodological differences, the slight variations in VTI values between our results and those previously reported may be attributed to the range of collateral segments selected for measurements. There is currently no accepted definition of the range of collateral segment, as its definition is related to the functional role during an occlusive event. For the consistency within measurements in our study, we followed the branching orders arterioles (e.g. the start point of measuring on the MCA side is at the last bifurcation of M1 segment with equal or similar sized trunks, and that one or both trunks are connected to ACA as collateral).

The mechanisms underlying age-related increase in artery tortuosity in aging remains unclear, but it is well hypothesized that structural alteration in the vessel wall plays a role in the early stage of tortuosity development (Han, 2012). As aging begins, smooth muscle cells (SMCs) progressively migrate from the tunica media to accumulate into the intima, and subsequently impair the integrity of the elastic membrane in the intima (Yildiz, 2007). Fracturing of the elastin fibers would lead to a reduction in elasticity, resulting in stiffening

of the vessel wall. As a result of the arterial stiffening, pulsatile blood pressure in the vessel lumen would become elevated, giving rise to vessel buckling to initiate tortuosity development (Kohn et al., 2015).

The fragmentation of elastin, which has been reported in the artery wall of aged subjects, has been considered a cause of the vessel lengthening and tortuosity progression (Sugawara et al., 2008). As a result, tortuosity increases the vessel length, and with each turn and loop there is a loss of kinetic energy that potentially reduces the flow speed in these vessels (Moody et al., 1991). While mild increase of vessel tortuosity may be asymptomatic, severe tortuosity developed with aging can significantly reduce conductance ability of the blood vessels and diminish cerebral perfusion; hence, producing focal ischemic lesion and cellular damage in the downstream tissue (Moody et al., 1991; Spangler et al., 1994). Tortuous penetrating arterioles in the white matter, for instance, are found to be a critical contributing factor to neurodegeneration in a subset of leukoaraiosis (LA) (Thore et al., 2007). In another case, augmented tortuosity in the cerebral pial arterioles can cause collateral rarefaction, which could increase blood flow resistance during arteriogenesis and contribute to a more severe ischemic stroke phenotype in older subjects (Faber et al., 2011). In addition to the coiling, looping, and spiraling profiles of blood vessels, the increased tortuosity is also associated with a greatly expanded Virchow-Robin perivascular space where amyloid movement occurs (Nicoll et al., 2004). The enlarged perivascular space could disrupt the drainage of amyloid deposits, contributing to the age-associated AD pathology (Brown et al., 2000).

Though tortuosity is found to be an important vascular factor contributing to various age-related pathological conditions, however, it is neither necessary nor sufficient to produce an LA or AD (Thore et al., 2007). A number of other vascular factors are critically involved in aging and the potential disease pathogenesis, which were also revealed in this study by OCTA as discussed in the following sections.

4.1.2 Aging-related capillary loss—The distance that oxygen can diffuse from blood into oxygen-consuming tissue is limited (Gagnon et al., 2016). The metabolically demanding nature of the brain means, therefore, that it must be supplied by a dense network of microvessels, so that each point in the tissue is within a distance of oxygen diffusion from the nearest blood vessel. A decrease in microvascular density may increase the risk of tissue hypoxia, and may reduce the oxygen extraction efficiency during functional activity (Hirsch et al., 2012). In comparison with the scarcity of systemic studies conducted for the investigation of arterial tortuosity during normal aging, the microvascular density changes through aging has attracted sizable interest. Collective evidence from 37 earlier studies have revealed an age-related vascular density decrease in both aging animals and human post-mortem (Brown and Thore, 2011). More specifically, an 8% to 43% reduction in capillary numbers (Amenta et al., 1995; Jucker et al., 1990; Knox and Oliveira, 1980; Villena et al., 2003; Wilkinson et al., 1981) and a 12% to 39 % reduction in capillary density (Burns et al., 1981; Casey and Feldman, 1985; Hinds and McNelly, 1982; Sonntag et al., 1997) were observed in brain of aged rats (22 to 31-month-old), and a decrease in capillary density of 16% to 50 % was measured from healthy aged human subjects (age 79 to 90) compared with younger subjects (age 49 to 57) (Abemethy et al., 1993; Bell and Ball, 1981; Brown et al.,

2000; Buée et al., 1994; Mann et al., 1986). Recently through the imaging of fluorescein isothiocyanate-dextran (FITC) dye-labeled cerebral capillary vessels using TPM in anesthetized rats, Desjardin *et al.* (2014) observed 20% decrease in capillary density in older rats. In the current study, capillary density was measured *in vivo* in the brains of anesthetized mice with OCTA without the need for exogenous contrast agents. The VAD of young and aged animals were measured as 0.40±0.05 and 0.34±0.08, respectively, which revealed an age-associated reduction in capillary density by 15%. Although the values from two groups were close, the difference is statistically significant ($p<0.01$) and has important implication on capillary flow dynamics and potentially brain oxygen extraction efficiency. In our penetrating vessel measurement by DOMAG, we surprisingly found little differences in arterial velocity between young and old groups, while capillary velocity was measured 21% in the old animals from capillary velocimetry measurement. We therefore speculate such dramatic increase in downstream flow velocity may be attributed, at least in part, to capillary density reduction.

Despite a lack of clear consensus concerning the causes of capillary loss, previous studies have suggested that age-dependent microvascular dropout may be associated with a decline in amplitude of pulsatile secretion of growth hormone (GH) and the resulting decrease in plasma levels of insulin-like growth factor 1 (IGF-1) with aging (Sonntag et al., 1997). Both GH and IGF-1 are responsible for the regulation of vascular growth, maintenance, and remodeling (Khan et al., 2002), and with advancing age, the secretion of these hormones is reduced, depressing the vascular regulation necessary for maintenance of downstream microvasculature, resulting in a progressive loss of microvessels. Furthermore, aging is associated with increasing blood pressure, and hypertension is known to cause vessel rarefaction (Sokolova et al., 1985; Gligorsky, 2010).

Although the causal relationship between capillary loss and neurodegeneration is still debatable, the possible contribution of microvascular deficiencies to aged brain as well as aged-related pathologies in cerebral vasculature and function (Farkas and Luiten, 2001; Fischer et al., 1990), could be studied under OCTA to enhance a comprehensive understanding of CBF reduction in these conditions.

4.1.3 CBF modification in the aging brain—The energy requirement of the brain is met almost exclusively by the oxidative metabolism of glucose, which is delivered to local neuron cells through blood vessels by continuous and sufficient CBF (Gagnon et al., 2016). Given that CBF is maintained and regulated by the coordinated efforts of interconnected blood vessels, including cerebral arteries, arterioles and capillaries (Kisler et al., 2017), age-related modifications in the arterial morphology and capillary density undoubtedly impact both resting state CBF and the ability to adjust blood flow during neuronal activities. The latter hemodynamic feature, also referred to as regional CBF (rCBF) change during functional activation, is coupled with the cerebral metabolic rate of oxygen ($CMRO_2$) in a disproportionate manner (Paulson et al., 2010), which creates a contrast signal that can be detected by fMRI (Ances et al., 2009) or PET (Aanerud et al., 2012).

Numerous studies have utilized flow-metabolism signals to investigate rCBF change with aging in human brains. Among those investigations, an age-related rCBF reduction was

reported with both young and old comparison studies (Ances et al., 2009; Bertsch et al., 2009) and correlative studies between rCBF and life time (Aanerud et al., 2012; Chen et al., 2011; Schultz et al., 1999). Although useful for the assessment of CBF involvement in brain function and performance during aging, these measurements only revealed relative changes in rCBF with respect to local cerebral metabolic rates. An absolute CBF from single arterioles was unobtainable by these imaging modalities, which fails to establish an association between the magnitudes of vascular structure modification with *in vivo* blood flow changes in the resting brain during vascular aging. On the other hand, studies using transcranial Doppler sonography (Demirkaya et al., 2008; Krejza et al., 1999) has successfully examined the blood flow velocity in basal cerebral arteries in the resting human brain, and observed decreased blood flow velocity with increasing age. In our current study, we applied the Doppler principle in OCTA technology to measure the velocity in penetrating vessels in mouse brain. The high-resolution vessel velocity maps produced by DOMAG also provided an ability of PA/RV flow area quantification, from which arteriole and venule CBF (mm^3/s) of a cortical region can be obtained by velocity (mm/s) × area (mm^2). In general, venules flow slower than arterioles (Fig. 5(d)), but with great number of branches and larger surface areas (Fig. 5(e)) than arterioles. The total flow volume of PA and RV almost equals to each other within each group (Fig. 5(f)) as an implication of flow conservation, which validate the accuracy of DOMAG measurements on CBF. We compared the velocity, flow area, and CBF between young and old groups (N=8). Interestingly, mean velocities of both arterioles and venules are not significantly different between two age groups. The flow area (cross section size), though, is significantly decreased in older animals, by 35% ($p<0.05$) in PA and 32% ($p<0.05$) in RV, which indicates reductions in vessel diameter and vessel population in the older animals. Such change has significant effect on the CBF. As a result, there is a 33% statistically significant reduction ($p<0.01$) in PA total flow, and 31% statistically significant reduction ($p<0.01$) in RV total flow.

Owing to the joint application of Doppler velocity measurements and OCTA, resting CBF can be evaluated concurrently with quantitative vessel tortuosity and density assessment *in vivo* through one-platform imaging. The CBF profile obtained here may be used as an important parameter to assess the wellness of neurovascular system. Together with a comprehensive evaluation on structural parameters, it may facilitate a discovery of critical thresholds in vascular modifications during aging, of which the magnitude of change is not secondary to normal aging but may instead indicate impending pathologies.

4.1.4 Capillary velocity heterogeneity development during aging—

The capillary flow pattern, a hemodynamic parameter separated from CBF, plays an equally critical role in the dynamics of tissue oxygenation and neuron functions (Gagnon et al., 2016; Jespersen and Østergaard, 2012). An essential imaging feature offered by our OCTA, aside from its ability to measure CBF in arterioles, is the capability of quantitatively analyzing the RBC speed and distribution from a large array of capillary vessels that no other current imaging techniques can achieve.

The significance of the spatiotemporal distribution of RBC speed within the capillary bed for normal brain function and pathology development has been vigorously reported in recent years. According to a model established by Jespersen & Østergaard (2012), higher capillary

transit time heterogneity (CTH), especially at shorter transit times (higher speeds), results in lower oxygen delivery to tissue relative to homogenous transit times across capillary vessels. The progressive development of CTH suspected with aging, therefore, is thought to have a casusative role in cognitive impairment with advancing age (Østergaard et al., 2013, 2015). Comparatively speaking, however, little information can be cited referring to the relevance of capillary heterogeneity to aging due to the inherent challenges associated with *in vivo* imaging of single-file, rapidly moving RBCs in capillary vessels. To our knowledge, only one study, using high-speed TMP, has reported capillary velocity and heterogeneity differences between young and old rats from scanning an average number of 38 (12~93) capillaries in the S1 cortex of each brain, which revealed a 48% and 43% increase in RBC mean velocity and spatial heterogeneity (standard deviation), respectively, within the aged group (Desjardins et al., 2014). From their study, however, if excluding the animals with less than 20 measured capillaries, in which the samples are too few for adequate heterogeneity evaluation, age-related difference in heterogeneity would not be statistically significant. Applying the OCTA velocimetry in this aging study, we targeted at the dynamic signal generated from RBC movements within the capillary bed and analyzed ~40,000 frequency-derived RBC velocities within each 3-D tissue volume obtained from the resting S1 cortex of young and old mice. We showed, with statistical confidence, a 21% increase in the mean capillary velocity ($p<0.05$) (Fig. 6(g)) and a 19% increase in heterogeneity ($p<0.05$) (Fig. 6(h)) in the old mice, which revealed, for the first time, an age-related significant difference in cerebral capillary velocity heterogeneity *in vivo*. Moreover, the 3-D imaging of such large quantities of capillaries was achieved within minutes, which makes it feasible to investigate the on-site hemodynamic response, known as capillary flow homogenization (Li et al., 2018), during stimulus-evoked neuronal activity. How aging impacts functional hyperemia or neurovascular coupling warrants further investigation.

4.2 Study limitations

Several limitations from the technical perspective of OCT imaging will be addressed. First, the range of imaging depth for capillary density and velocity measurements was limited to 300 μm from the cortical surface (corresponding to layers I, II, and III of the cortex). Such choice was made to eliminate a bias in measuring at deeper cortical layers due to multiple-scattering that might cause signal attenuation and resolution degradation. Furthermore, due to such limitation, only pial arterioles were taken as a representative vessel group for tortuosity evaluation. To further investigate vessel tortuosity in deeper brain layers and its causative role in white matter diseases, histological analyses are required. Additionally, in capillary velocimetry method, a linear relationship between ED-based frequency and mean capillary transit velocity was used based on validation on simple network phantom experiments. An improved correlation between frequency and RBC velocity considering the interwoven capillary network and the size and shape of RBC remains to be fully explored. However, neither imaging limitations here are thought to be significant enough to invalidate our comparisons between young and old groups in the current study.

The use of inhalational isoflurane has been shown to influence animal physiology parameters. Overall, the anesthetized animals tend to have increased heart rate (HR), reduced blood pressure (BP), and could potentially develop hypercapnia over time (Janssen

et al., 2004; Schlünzen et al., 2006; Vutskits and Xie, 2016). In this study, the level of isoflurane was controlled at 1.5% v/v throughout, which is at the level proven in a previous study to yield stable blood pressure and heart rate values comparable to those observed in the animal's conscious state (Constantinides et al., 2011), and we monitored animal physiology parameters during the experiment as shown in Table 1. The HR and BP in the old group were on the lower side. One explanation for this could be that age reduces the amount of isoflurane needed (Matsuura et al., 2009), and as we kept the same level of isoflurane in both groups, the old mice might possibly be in a deeper anesthetic state compare to the young. The effect of isoflurane on heart and vascular function also depends on the level of oxygen (Constantinides et al., 2011). In our study, the SpO_2 was monitored, and maintained at ~96% with the use of air/oxygen gas mixture (0.8 L/min air and 0.2 L/min O_2), and there were no differences in SpO_2 between young and old groups, which rule out this variable from affecting physiology differences. The observed differences in physiology parameters (HR, BP) may have influences on the measured blood flow values (e.g. CBF and capillary velocity), which remains to be explored in the future study using awake mouse. Nonetheless, the differences in the level of anesthesia does not invalidate our main observations of age-associated differences in this study, especially in vascular structure, tortuosity, and capillary density. Further investigation may be warranted in comparing the OCTA measured parameters in young and aged mice under awake conditions to exclude the effect of isoflurane anesthesia on microcirculatory dynamics *in vivo* (Moeini et al., 2015).

5. CONCLUSION

In this study, we have systematically investigated age-associated changes in vascular features in mouse brains *in vivo* using a collection of OCTA based algorithms. From the micrometer resolution angiogram, an increased cerebral arterial tortuosity with a decreased capillary density in old mice was revealed simultaneously, which was consistent with previously published results. Alongside with vessel structure modification, changes in hemodynamic parameters, including decreased arterial CBF and increased capillary velocity and heterogeneity were uncovered within the older age group. OCTA presented a superior advantage for multi-feature evaluation using just one imaging platform. Such information would facilitate a comprehensive understanding of vascular aging and its involvement in the age-related neurovascular diseases.

Acknowledgement

The authors would like to thank Dr. Anthony J. Deegan for the critical proof reading during the preparation of the manuscript. This work was supported in part by research grants from National Heart, Lung and Blood Institute (R01HL093140), National Eye Institute (R01EY024158), Washington Research Foundation and an unrestricted fund from Research to Prevent Blindness, National Institutes of Health grant R01NS102886, and Veterans Affairs merit award I01BX002690. The funding organizations had no role in the design or conduct of this research.

Funding information

This work was supported in part by research grants from National Heart, Lung and Blood Institute (R01HL093140), National Eye Institute (R01EY024158), Washington Research Foundation and an unrestricted fund from Research to Prevent Blindness, National Institutes of Health grant R01NS102886, and Veterans Affairs merit award I01BX002690. The funding organizations had no role in the design or conduct of this research.

References

Aanerud J, Borghammer P, Chakravarty MM, Vang K, Rodell AB, Jónsdottir KY, Møller A, Ashkanian M, Vafaee MS, Iversen P, Johannsen P, Gjedde A, 2012 Brain energy metabolism and blood flow differences in healthy aging. J. Cereb. Blood Flow Metab. Off. J. Int. Soc. Cereb. Blood Flow Metab 32, 1177–1187.

Abernethy WB, Bell MA, Morris M, Moody DM, 1993 Microvascular density of the human paraventricular nucleus decreases with aging but not hypertension. Exp. Neurol. 121, 270–274. [PubMed: 8339778]

Amenta F, Cavallotti D, Del Valle M, Mancini M, Naves FJ, Vega JA, Zeng YC, 1995 Age-related changes in brain microanatomy: sensitivity to treatment with the dihydropyridine calcium channel blocker darodipine (PY 108-068). Brain Res. Bull. 36, 453–460. [PubMed: 7712207]

Ances BM, Liang CL, Leontiev O, Perthen JE, Fleisher AS, Lansing AE, Buxton RB, 2009 Effects of aging on cerebral blood flow, oxygen metabolism, and blood oxygenation level dependent responses to visual stimulation. Hum. Brain Mapp. 30, 1120–1132.

Attems J, Jellinger KA, 2014 The overlap between vascular disease and Alzheimer's disease - lessons from pathology. BMC Med. 12, 206. [PubMed: 25385447]

Baran U, Li Y, Wang RK, 2015 Vasodynamics of pial and penetrating arterioles in relation to arteriolo-arteriolar anastomosis after focal stroke. Neurophotonics 2, 025006. [PubMed: 26158010]

Bell MA, Ball MJ, 1981 Morphometric comparison of hippocampal microvasculature in ageing and demented people: diameters and densities. Acta Neuropathol. (Berl.) 53, 299–318. [PubMed: 7223373]

Berman RF, Goldman H, Altman HJ, 1988 Age-related changes in regional cerebral blood flow and behavior in Sprague-Dawley rats. Neurobiol. Aging 9, 691–696. [PubMed: 3062475]

Bertsch K, Hagemann D, Hermes M, Walter C, Khan R, Naumann E, 2009 Resting cerebral blood flow, attention, and aging. Brain Res. 1267, 77–88. [PubMed: 19272361]

Breteler MM, 2000 Vascular involvement in cognitive decline and dementia. Epidemiologic evidence from the Rotterdam Study and the Rotterdam Scan Study. Ann. N. Y. Acad. Sci. 903, 457–465. [PubMed: 10818538]

Brown WR, Moody DM, Thore CR, Challa VR, 2000 Cerebrovascular pathology in Alzheimer's disease and leukoaraiosis. Ann. N. Y. Acad. Sci. 903, 39–45. [PubMed: 10818487]

Brown WR, Moody DM, Thore CR, Challa VR, Anstrom JA, 2007 Vascular dementia in leukoaraiosis may be a consequence of capillary loss not only in the lesions, but in normalappearing white matter and cortex as well. J. Neurol. Sci. 257, 62–66. [PubMed: 17320909]

Brown WR, Thore CR, 2011 Review: Cerebral microvascular pathology in aging and neurodegeneration. Neuropathol. Appl. Neurobiol. 37, 56–74. [PubMed: 20946471]

Buée L, Hof PR, Bouras C, Delacourte A, Perl DP, Morrison JH, Fillit HM, 1994 Pathological alterations of the cerebral microvasculature in Alzheimer's disease and related dementing disorders. Acta Neuropathol. (Berl.) 87, 469–480. [PubMed: 8059599]

Bullitt E, Zeng D, Mortamet B, Ghosh A, Aylward SR, Lin W, Marks BL, Smith K, 2010 The effects of healthy aging on intracerebral blood vessels visualized by magnetic resonance angiography. Neurobiol. Aging 31, 290–300. [PubMed: 18471935]

Burns EM, Kruckeberg TW, Gaetano PK, 1981 Changes with age in cerebral capillary morphology. Neurobiol. Aging 2, 283–291. [PubMed: 7335147]

Casey MA, Feldman ML, 1985 Aging in the rat medial nucleus of the trapezoid body. III. Alterations in capillaries. Neurobiol. Aging 6, 39–46. [PubMed: 4000384]

Chen JJ, Rosas HD, Salat DH, 2011 Age-associated reductions in cerebral blood flow are independent from regional atrophy. NeuroImage 55, 468–478. [PubMed: 21167947]

Choi WJ, Li Y, Qin W, Wang RK, 2016 Cerebral capillary velocimetry based on temporal OCT speckle contrast. Biomed. Opt. Express 7, 4859–4873. [PubMed: 28018711]

Chu Z, Lin J, Gao C, Xin C, Zhang Q, Chen C-L, Roisman L, Gregori G, Rosenfeld PJ, Wang RK, 2016 Quantitative assessment of the retinal microvasculature using optical coherence tomography angiography. J. Biomed. Opt. 21, 66008. [PubMed: 27286188]

Constantinides C, Mean R, Janssen BJ, 2011 Effects of isoflurane anesthesia on the cardiovascular function of the C57BL/6 mouse. ILAR J. 52, e21–31. [PubMed: 21677360]

de la Torre JC, 1999 Critical threshold cerebral hypoperfusion causes Alzheimer's disease? Acta Neuropathol. (Berl.) 98, 1–8. [PubMed: 10412794]

Demirkaya S, Uluc K, Bek S, Vural O, 2008 Normal blood flow velocities of basal cerebral arteries decrease with advancing age: a transcranial Doppler sonography study. Tohoku J. Exp. Med. 214, 145–149. [PubMed: 18285672]

Desjardins M, Berti R, Lefebvre J, Dubeau S, Lesage F, 2014 Aging-related differences in cerebral capillary blood flow in anesthetized rats. Neurobiol. Aging 35, 1947–1955. [PubMed: 24612672]

Diaz-Otero JM, Garver H, Fink GD, Jackson WF, Dorrance AM, 2016 Aging is associated with changes to the biomechanical properties of the posterior cerebral artery and parenchymal arterioles. Am. J. Physiol. Heart Circ. Physiol. 310, H365–375. [PubMed: 26637558]

Efford N, 2000 Digital Image Processing: A Practical Introduction Using Java (with CD-ROM), 1st ed. Addison-Wesley Longman Publishing Co., Inc., Boston, MA, USA.

Faber JE, Zhang H, Lassance-Soares RM, Prabhakar P, Najafi AH, Burnett MS, Epstein SE, 2011 Aging causes collateral rarefaction and increased severity of ischemic injury in multiple tissues. Arterioscler. Thromb. Vasc. Biol. 31, 1748–1756. [PubMed: 21617137]

Farkas E, De Vos RA, Jansen Steur EN, Luiten PG, 2000 Are Alzheimer's disease, hypertension, and cerebrocapillary damage related? Neurobiol. Aging 21, 235–243. [PubMed: 10867208]

Farkas E, Luiten PG, 2001 Cerebral microvascular pathology in aging and Alzheimer's disease. Prog. Neurobiol. 64, 575–611. [PubMed: 11311463]

Fischer VW, Siddiqi A, Yusufaly Y, 1990 Altered angioarchitecture in selected areas of brains with Alzheimer's disease. Acta Neuropathol. (Berl.) 79, 672–679. [PubMed: 2360411]

Gagnon L, Smith AF, Boas DA, Devor A, Secomb TW, Sakadžić S, 2016 Modeling of Cerebral Oxygen Transport Based on In vivo Microscopic Imaging of Microvascular Network Structure, Blood Flow, and Oxygenation. Front. Comput. Neurosci 10. [PubMed: 26903851]

Goligorsky MS, 2010 Microvascular rarefaction. Organogenesis 6, 1–10. [PubMed: 20592859]

Han H-C, 2012 Twisted blood vessels: symptoms, etiology and biomechanical mechanisms. J. Vasc.

Helmchen F, Denk W, 2005 Deep tissue two-photon microscopy. Nat. Methods 2, 932–940. [PubMed: 16299478]

Heo S, Prakash RS, Voss MW, Erickson KI, Ouyang C, Sutton BP, Kramer AF, 2010 Resting hippocampal blood flow, spatial memory and aging. Brain Res. 1315, 119–127. [PubMed: 20026320]

Hinds JW, McNelly NA, 1982 Capillaries in aging rat olfactory bulb: a quantitative light and electron microscopic analysis. Neurobiol. Aging 3, 197–207. [PubMed: 7162549]

Hirsch S, Reichold J, Schneider M, Székely G, Weber B, 2012 Topology and hemodynamics of the cortical cerebrovascular system. J. Cereb. Blood Flow Metab. Off. J. Int. Soc. Cereb. Blood Flow Metab 32, 952–967.

Hofman A, Ott A, Breteler MM, Bots ML, Slooter AJ, van Harskamp F, van Duijn CN, Van Broeckhoven C, Grobbee DE, 1997 Atherosclerosis, apolipoprotein E, and prevalence of dementia and Alzheimer's disease in the Rotterdam Study. Lancet Lond. Engl 349, 151–154.

Hutchins GM, Miner MM, Bulkley BH, 1978 Tortuosity as an index of the age and diameter increase of coronary collateral vessels in patients after acute myocardial infarction. Am. J. Cardiol. 41, 210–215. [PubMed: 623014]

Janssen BJA, De Celle T, Debets JJM, Brouns AE, Callahan MF, Smith TL, 2004 Effects of anesthetics on systemic hemodynamics in mice. Am. J. Physiol. Heart Circ. Physiol. 287, H1618–1624. [PubMed: 15155266]

Jespersen SN, 0stergaard L, 2012 The roles of cerebral blood flow, capillary transit time heterogeneity, and oxygen tension in brain oxygenation and metabolism. J. Cereb. Blood Flow Metab. Off. J. Int. Soc. Cereb. Blood Flow Metab 32, 264–277.

Jucker M, Bättig K, Meier-Ruge W, 1990 Effects of aging and vincamine derivatives on pericapillary microenvironment: stereological characterization of the cerebral capillary network. Neurobiol. Aging 11, 39–46. [PubMed: 2325815]

Kang H-M, Sohn I, Jung J, Jeong J-W, Park C, 2016 Age-related changes in pial arterial structure and blood flow in mice. Neurobiol. Aging 37, 161–170. [PubMed: 26460142]

Khan AS, Sane DC, Wannenburg T, Sonntag WE, 2002 Growth hormone, insulin-like growth factor-1 and the aging cardiovascular system. Cardiovasc. Res. 54, 25–35. [PubMed: 12062358]

Kim AY, Chu Z, Shahidzadeh A, Wang RK, Puliafito CA, Kashani AH, 2016 Quantifying Microvascular Density and Morphology in Diabetic Retinopathy Using Spectral-Domain Optical Coherence Tomography Angiography. Invest. Ophthalmol. Vis. Sci. 57, OCT362–370. [PubMed: 27409494]

Kisler K, Nelson AR, Montagne A, Zlokovic BV, 2017 Cerebral blood flow regulation and neurovascular dysfunction in Alzheimer disease. Nat. Rev. Neurosci. 18, 419–434. [PubMed: 28515434]

Knox CA, Oliveira A, 1980 Brain aging in normotensive and hypertensive strains of rats. III. A quantitative study of cerebrovasculature. Acta Neuropathol. (Berl.) 52, 17–25. [PubMed: 7435153]

Kohn JC, Lampi MC, Reinhart-King CA, 2015 Age-related vascular stiffening: causes and consequences. Front. Genet 6. [PubMed: 25688259]

Krejza J, Mariak Z, Walecki J, Szydlik P, Lewko J, Ustymowicz A, 1999 Transcranial color Doppler sonography of basal cerebral arteries in 182 healthy subjects: age and sex variability and normal reference values for blood flow parameters. AJR Am. J. Roentgenol. 172, 213–218. [PubMed: 9888770]

Li Y, Baran U, Wang RK, 2014 Application of thinned-skull cranial window to mouse cerebral blood flow imaging using optical microangiography. PLoS ONE 9, 1–13.

Li Y, Wei W, Wang RK, 2018 Capillary flow homogenization during functional activation revealed by optical coherence tomography angiography based capillary velocimetry. Sci. Rep. 8, 4107. [PubMed: 29515156]

Liang C-P, Wu Y, Schmitt J, Bigeleisen PE, Slavin J, Jafri MS, Tang C-M, Chen Y, 2013 Coherence-gated Doppler: a fiber sensor for precise localization of blood flow. Biomed. Opt. Express 4, 760–771. [PubMed: 23667791]

Lynch CD, Cooney PT, Bennett SA, Thornton PL, Khan AS, Ingram RL, Sonntag WE, 1999 Effects of moderate caloric restriction on cortical microvascular density and local cerebral blood flow in aged rats. Neurobiol. Aging 20, 191–200. [PubMed: 10537028]

Mann DM, Eaves NR, Marcyniuk B, Yates PO, 1986 Quantitative changes in cerebral cortical microvasculature in ageing and dementia. Neurobiol. Aging 7, 321–330. [PubMed: 3785532]

Matsuura T, Oda Y, Tanaka K, Mori T, Nishikawa K, Asada A, 2009 Advance of age decreases the minimum alveolar concentrations of isoflurane and sevoflurane for maintaining bispectral index below 50. British Journal of Anaesthesia 102, 331–335. [PubMed: 19168857]

Moeini M, Tabatabaei MS, Belanger S, Avti P, Castonguay A, Pouliot P, Lesage F, 2015 Effects of anesthesia on the cerebral capillary blood flow in young and old mice. Presented at the Multiphoton Microscopy in the Biomedical Sciences XV, International Society for Optics and Photonics, p. 932929.

Moody DM, Santamore WP, Bell MA, 1991 Does tortuosity in cerebral arterioles impair down-autoregulation in hypertensives and elderly normotensives? A hypothesis and computer model. Clin. Neurosurg. 37, 372–387. [PubMed: 2009699]

Nicoll JAR, Yamada M, Frackowiak J, Mazur-Kolecka B, Weller RO, 2004 Cerebral amyloid angiopathy plays a direct role in the pathogenesis of Alzheimer's disease. Pro-CAA position statement. Neurobiol. Aging 25, 589–597; discussion 603–604. [PubMed: 15172734]

Nishimura N, Schaffer CB, Friedman B, Lyden PD, Kleinfeld D, 2007 Penetrating arterioles are a bottleneck in the perfusion of neocortex. Proc. Natl. Acad. Sci. U. S. A. 104, 365–370. [PubMed: 17190804]

Østergaard L, Aamand R, Gutiérrez-Jiménez E, Ho Y-CL, Blicher JU, Madsen SM, Nagenthiraja K, Dalby RB, Drasbek KR, Møller A, Brændgaard H, Mouridsen K, Jespersen SN, Jensen MS, West MJ, 2013 The capillary dysfunction hypothesis of Alzheimer's disease. Neurobiol. Aging 34, 1018–1031. [PubMed: 23084084]

Østergaard L, Jespersen SN, Engedahl T, Gutiérrez Jiménez E, Ashkanian M, Hansen MB, Eskildsen S, Mouridsen K, 2015 Capillary dysfunction: its detection and causative role in dementias and stroke. Curr. Neurol. Neurosci. Rep. 15, 37. [PubMed: 25956993]

Paulson OB, Hasselbalch SG, Rostrup E, Knudsen GM, Pelligrino D, 2010 Cerebral blood flow response to functional activation. J. Cereb. Blood Flow Metab. Off. J. Int. Soc. Cereb. Blood Flow Metab 30, 2–14.

Schlünzen L, Cold GE, Rasmussen M, Vafaee MS, 2006 Effects of dose-dependent levels of isoflurane on cerebral blood flow in healthy subjects studied using positron emission tomography. Acta Anaesthesiol. Scand. 50, 306–312. [PubMed: 16480463]

Schultz SK, O'Leary DS, Boles Ponto LL, Watkins GL, Hichwa RD, Andreasen NC, 1999 Age-related changes in regional cerebral blood flow among young to mid-life adults. Neuroreport 10, 2493–2496. [PubMed: 10574358]

Shi L, Qin J, Reif R, Wang RK, 2013 Wide velocity range Doppler optical microangiography using optimized step-scanning protocol with phase variance mask. J. Biomed. Opt. 18, 106015. [PubMed: 24165741]

Sokolova IA, Manukhina EB, Blinkov SM, Koshelev VB, Pinelis VG, Rodionov IM, 1985 Rarefiction of the arterioles and capillary network in the brain of rats with different forms of hypertension. Microvasc. Res. 30, 1–9 [PubMed: 4021832]

Sonntag WE, Lynch CD, Cooney PT, Hutchins PM, 1997 Decreases in cerebral microvasculature with age are associated with the decline in growth hormone and insulin-like growth factor 1. Endocrinology 138, 3515–3520. [PubMed: 9231806]

Spangler KM, Challa VR, Moody DM, Bell MA, 1994 Arteriolar tortuosity of the white matter in aging and hypertension. A microradiographic study. J. Neuropathol. Exp. Neurol 53, 22–26. [PubMed: 8301316]

Srinivasan VJ, Sakadžić S, Gorczynska I, Ruvinskaya S, Wu W, Fujimoto JG, Boas DA, 2010 Quantitative cerebral blood flow with optical coherene tomography. Opt. Express 18, 2477–2479. [PubMed: 20174075]

Sugawara J, Hayashi K, Yokoi T, Tanaka H, 2008 Age-associated elongation of the ascending aorta in adults. JACC Cardiovasc. Imaging 1, 739–748. [PubMed: 19356510]

Thore CR, Anstrom JA, Moody DM, Challa VR, Marion MC, Brown WR, 2007 Morphometric Analysis of Arteriolar Tortuosity in Human Cerebral White Matter of Preterm, Young, and Aged Subjects 66, 337–345.

Thore CR, Anstrom JA, Moody DM, Challa VR, Marion MC, Brown WR, 2007 Morphometric analysis of arteriolar tortuosity in human cerebral white matter of preterm, young, and aged subjects. J. Neuropathol. Exp. Neurol. 66, 337–345. [PubMed: 17483690]

Villena A, Vidal L, Díaz F, Pérez De Vargas I, 2003 Stereological changes in the capillary network of the aging dorsal lateral geniculate nucleus. Anat. Rec. A. Discov. Mol. Cell. Evol. Biol. 274, 857–861. [PubMed: 12923896]

Vutskits L, Xie Z, 2016 Lasting impact of general anaesthesia on the brain: mechanisms and relevance. Nat. Rev. Neurosci. 17, 705–717. [PubMed: 27752068]

Wang H, Shi L, Qin J, Yousefi S, Li Y, Wang RK, 2014 Multimodal optical imaging can reveal changes in microcirculation and tissue oxygenation during skin wound healing. Lasers Surg. Med. 46, 470–478. [PubMed: 24788236]

Wang RK, An L, 2009 Doppler optical micro-angiography for volumetric imaging of vascular perfusion in vivo. Opt. Express 17, 8926–8940. [PubMed: 19466142]

Wang RK, Jacques SL, Ma Z, Hurst S, Hanson SR, Gruber A, 2007 Three dimensional optical angiography. Opt. Express 15, 4083–4097. [PubMed: 19532651]

Wang RK, Zhang Q, Li Y, Song S, 2017 Optical coherence tomography angiography-based capillary velocimetry. J. Biomed. Opt. 22, 66008. [PubMed: 28617921]

Wilkinson JH, Hopewell JW, Reinhold HS, 1981 A quantitative study of age-related changes in the vascular architecture of the rat cerebral cortex. Neuropathol. Appl. Neurobiol. 7, 451–462. [PubMed: 7329517]

Xu X, Wang B, Ren C, Hu J, Greenberg DA, Chen T, Xie L, Jin K, 2017 Age-related Impairment of Vascular Structure and Functions. Aging Dis. 8, 590–610. [PubMed: 28966804]

Yildiz O, 2007 Vascular smooth muscle and endothelial functions in aging. Ann. N. Y. Acad. Sci. 1100, 353–360. [PubMed: 17460198]

Zhi Z, Cepurna W, Johnson E, Shen T, Morrison J, Wang RK, 2011 Volumetric and quantitative imaging of retinal blood flow in rats with optical microangiography. Biomed. Opt. Express 2, 579–591. [PubMed: 21412463]

HIGHLIGHTS

- Quantitative findings of age-associated vascular changes revealed from single-platform imaging
- Arterial tortuosity increases by 14% with older age.
- Capillary density decreases by 15% with older age.
- Cerebral blood flow reduces by 33% with older age.
- Capillary velocity increases by 21% and velocity heterogeneity increases by 19% with older age.

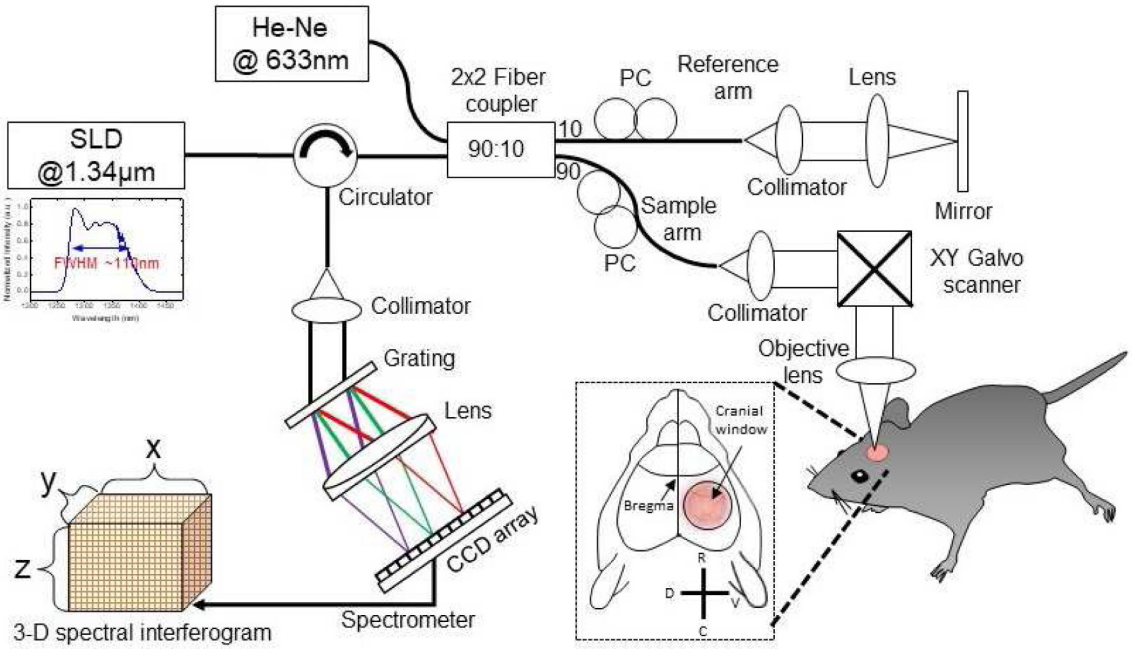

Fig. 1.

A schematic representation of the 1300 nm SD-OCT system setup. All OCTA scanning protocols (described in Section 2.3) were performed on this single OCT platform. A 5-mm diameter round glass cranial window was created on the right parietal bone at 1 mm posterior and lateral to the bregma. Scale bar orientation: C, caudal; D, dorsal; He-Ne,helium neon laser; PC, polarizer controller; R, rostral; SLD, super-luminescent diode; V, ventral.

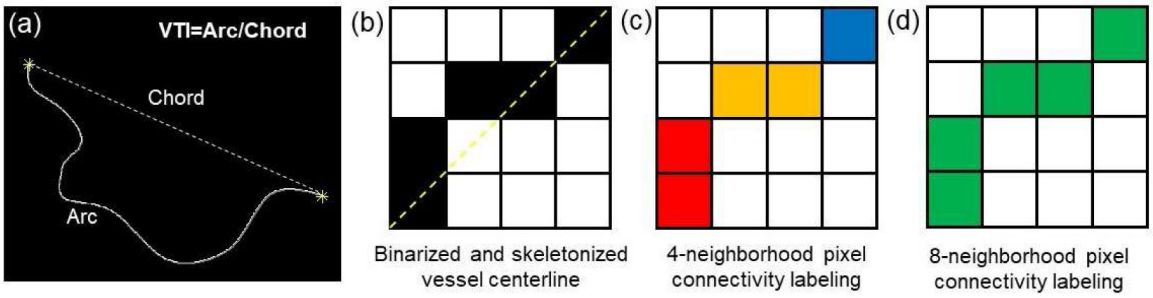

Fig. 2.

Method used for vessel tortuosity measurements. (A) A sketch demonstrating the definition of vessel tortuosity index (VTI) as a length of vessel (arc) divided by a length of straight line (chord) connecting its end points (yellow asterisks). (B) A 5-pixel example of binary vessel segment, with chord distance marked in yellow dashed line. (C) Pixel connectivity labeling for 4-neighborhood pixels. If the 4-neihgborhood condition was not met, the pixel path changes with a different label color. Therefore, 3 paths are labeled with 3 different colors: red, yellow, and blue. (D) Pixel connectivity labeling for 8-neighborhood pixels. In this case, all 5 pixels are 8-neighborhood pixels, touching one of the neighbor pixel's edges or corners; thus giving 1 complete pixel path labeled with green.

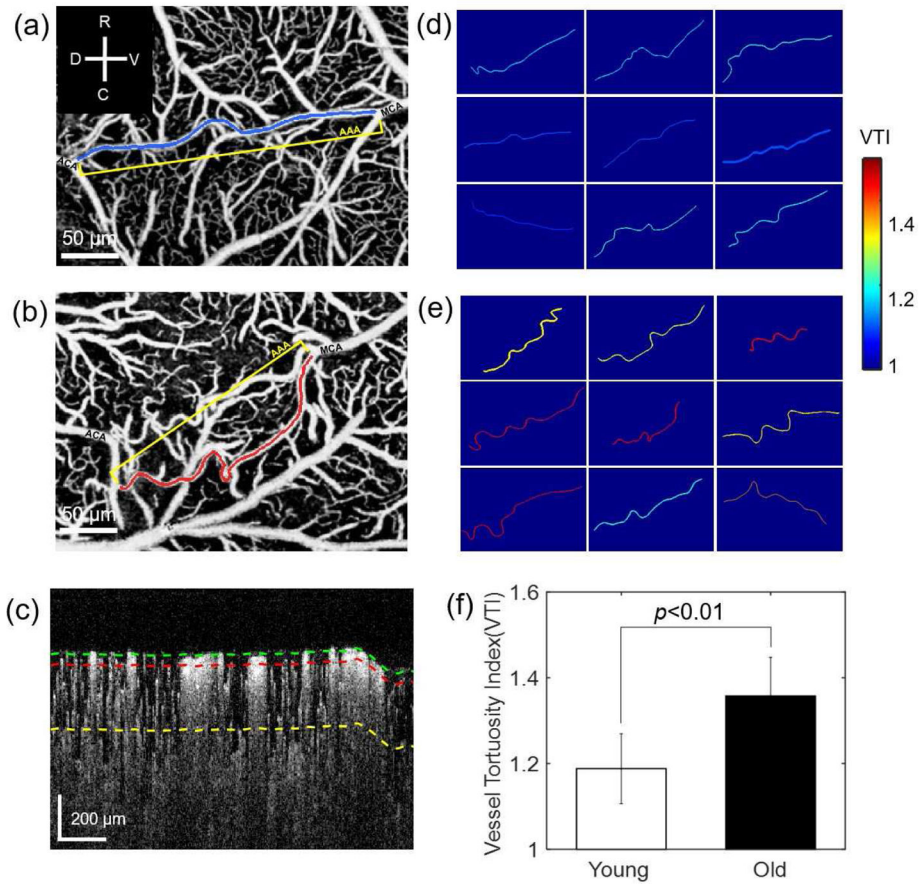

Fig. 3.

Comparison of cerebral pial collateral vessel tortuosity. (A) and (B) are angiograms of the young and old mice, respectively, obtained from *en face* maximum intensity projection (MIP) of 3-D OMAG datasets within 50 μm thick slab between the green and red dotted lines shown in B-scan flow cross section image (C). The green line in (C) marks the cortical surface, while the red and yellow lines are located at the depths of 50 and 300 μm from the cortical surface, respectively. On the angiogram (A) and (B), the selected AAA segments between MCA and ACA are highlighted with false colors. The colors represent calculated VTI values as indicated on the color bar. A total of 9 AAA segments were measured in each group as shown in (D) young and (E) old mice. (F) Comparison of VTI between young and old groups. The values are mean ± std. (standard deviation of group mean, N = 9 segments per group).

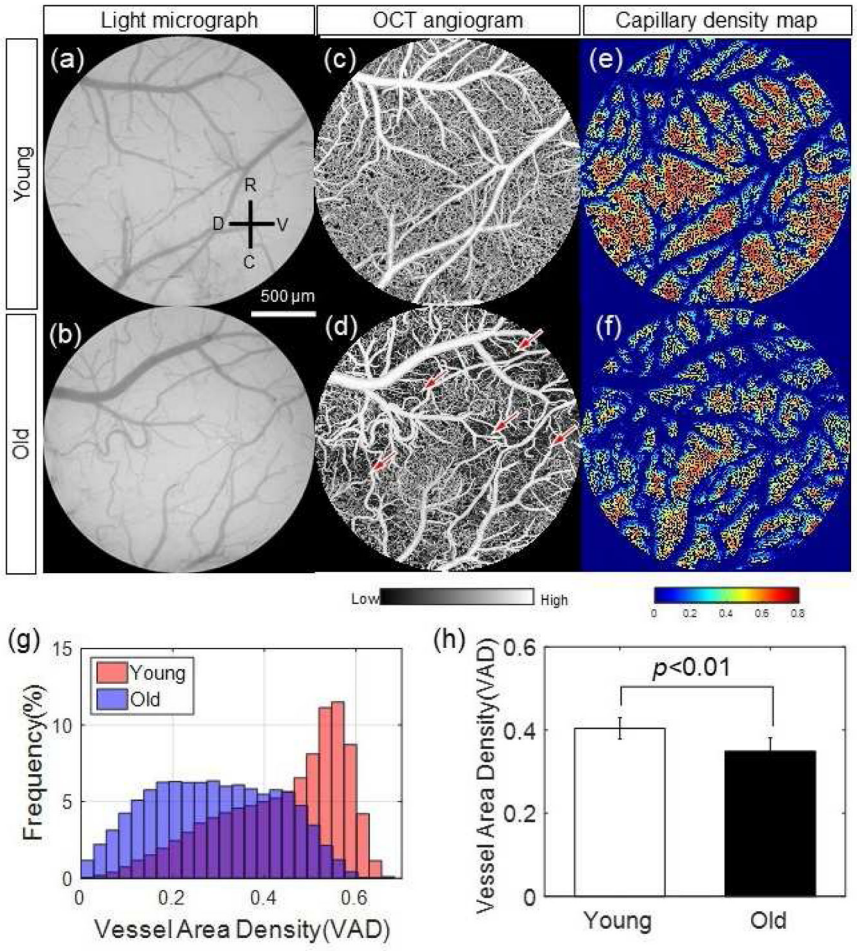

Fig. 4.

Comparison of the cerebral capillary vessel density. (A and B) Bright-field microscopy images of young and old mice, respectively, in a 2.5 mm × 2.5 mm region within cranial window. (C and D) OMAG angiograms corresponding to (A and B), respectively, constructed by *en face* MIP within 300 μm thick slab from cortical surface. Red arrows in (D) point out a suspected regional capillary rarefaction in the old animal. (C and F) are color index-coded VAD maps of young and old mice, respectively. (G) The VAD frequency histogram distributions of young (coral) and old mice (blue). (H) Comparison of VAD between young and old mice. The values are mean ± std. (standard deviation of group mean, N = 8 animals per group).

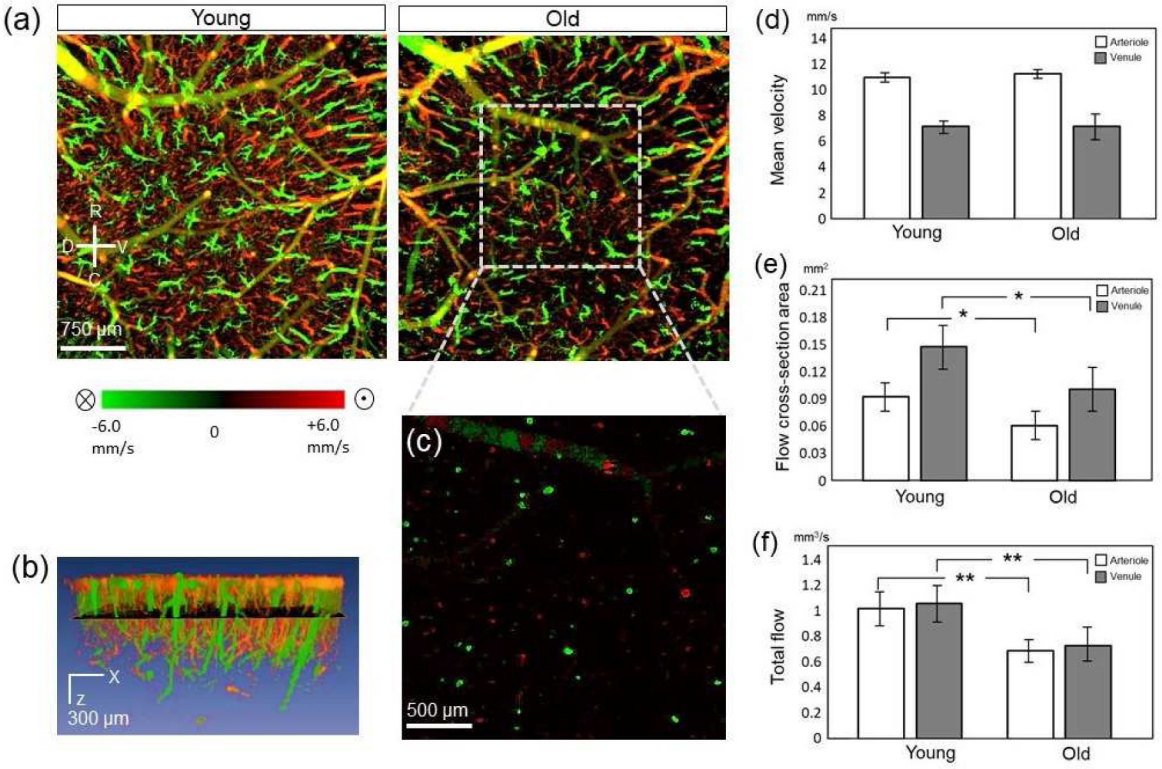

Fig. 5.

CBF and PA/RV parameter comparisons. (A) Bidirectional axial velocity maps of young and old mice generated by *en face* MIP of 3-D DOMAG datasets within 300 μm thick slab from cortical surface. Color bar represents RBC axial velocity of the flow descending (negative, green) and rising from (positive, red) the brain in a range of ±6.0 mm/s for the displayed maps. The yellow color was generated from a mix of green and red signals from the projection effect. (B) 3-D visualization of descending and ascending vessels within the white squared region in (A). (C) Orthogonal slice from (B), at an x-y plane ~50 μm below cortical surface. The green and red dots represent the descending arterioles and rising venules within the selected x-y plane, respectively. Green and red dots shown in (C) are cross sections of arteriole and venule flows. (D), (E) and (F) Comparisons of mean velocity, flow area, and total flow values, respectively, in unit region (1 mm^2) between young and old animals in both penetrating arterioles and venules. Values are mean ± std. (standard deviation of group mean). *$p < 0.05$; **$p < 0.01$.

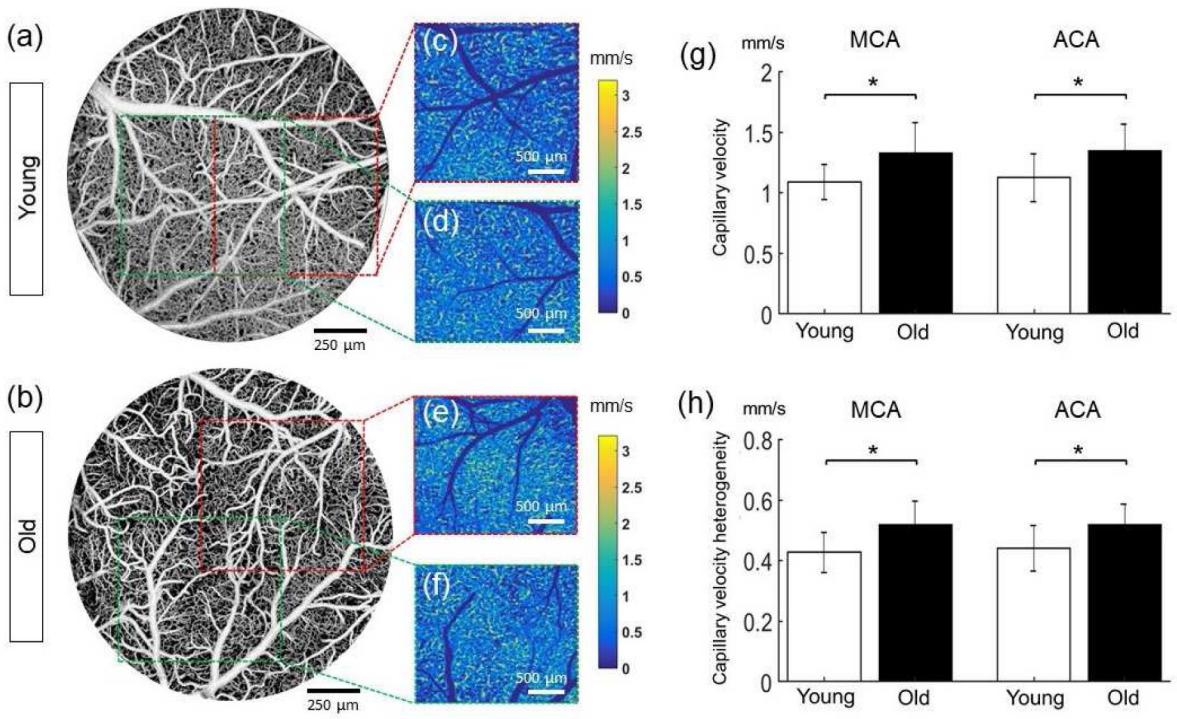

Fig. 6.

Capillary flow velocity and heterogeneity quantification. (A and B) Standard OMAG angiograms of young and old mice, respectively. Red and green squares indicated the regions where velocimetry was performed at MCA and ACA locations, respectively. (C–F) Capillary velocity maps generated by *en face* projection of 3-D frequency signal with 300 μm thick slab from the cortical surface. Color bar represents RBC velocity (0~3 mm/s). (G) Capillary mean velocity comparison between young and old mice. Values are mean ± std. (standard deviation of the group mean). *$p < 0.05$ in both MCA and ACA region. (H) Capillary velocity heterogeneity comparison between young and old mice. Values are mean ± std. *$p < 0.05$ and $p = 0.05$ at MCA and ACA region, respectively.

Table 1.

Measured physiology parameters. Values shown are mean ± std. (standard deviation of group mean). The asterisk symbols and bold text denote statistically significant difference (p<0.05) between the two groups.

Parameter	**Group**	
	Young	**Old**
Number of animals	8	8
Heart rate (beats/min)	**483 ± 52***	**435 ± 47***
Respiratory rate (breaths/min)	92 ± 10	87 ± 11
Diastolic arterial pressure (mm Hg)	**68 ± 12***	**61 ± 10***
Systolic arterial pressure (mm Hg)	**81 ± 14***	**72 ± 11***
Blood oxygen saturation (SpO_2%)	96 ± 1	96 ± 1

Table 2.

Characteristic age-associated changes. Values shown are mean ± std. (standard deviation of the mean in each animal among the same group). The asterisk symbols and bold text denote statistically significant difference between the 2 groups

Parameter	Group		Change (young → old)
	Young	Old	
Vessel tortuosity index (VTI)	**1.19 ± 0.07**	**1.36 ± 0.09**	**+14%** **
Capillary density (VAD)	**0.40 ± 0.05**	**0.34 ± 0.08**	**−15%** **
PA cerebral blood flow (mm^3/s)	**1.03 ± 0.04**	**0.69 ± 0.03**	**−33%** **
Capillary mean velocity (mm/s)	**1.11 ± 0.17**[a]	**1.34 ± 0.23**[a]	**+21%** *
Capillary velocity heterogeneity (mm/s)	**0.44 ± 0.07**[a]	**0.52 ± 0.08**[a]	**+19%** *, [b]

[a] Values are averaged from the measurements in ACA and MCA territories.

[b] p=0.052 for capillary velocity heterogeneity measured in ACA regions.

* p<0.05,

** p<0.01 from two-tailed t test.